

Localization of Protein Complex Bound Ligands by Surface-Induced Dissociation High-Resolution Mass Spectrometry

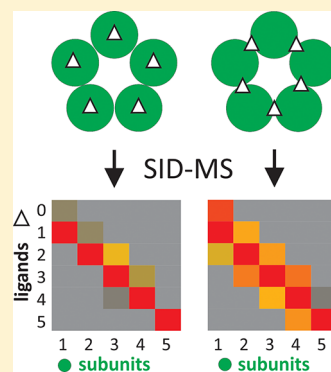
Florian Busch,^{†,‡} Zachary L. VanAernum,^{†,‡} Yue Ju,^{†,‡} Jing Yan,[†] Joshua D. Gilbert,[†] Royston S. Quintyn,[†] Marshall Bern,[‡] and Vicki H. Wysocki^{*,†}

[†]Department of Chemistry and Biochemistry, The Ohio State University, Columbus, Ohio 43210, United States

[‡]Protein Metrics Inc., 20863 Stevens Creek Blvd., Suite 450, Cupertino, California 95014, United States

Supporting Information

ABSTRACT: Surface-induced dissociation (SID) is a powerful means of deciphering protein complex quaternary structures due to its capability of yielding dissociation products that reflect the native structures of protein complexes in solution. Here we explore the suitability of SID to locate the ligand binding sites in protein complexes. We studied C-reactive protein (CRP) pentamer, which contains a ligand binding site within each subunit, and cholera toxin B (CTB) pentamer, which contains a ligand binding site between each adjacent subunit. SID dissects ligand-bound CRP into subcomplexes with each subunit carrying predominantly one ligand. In contrast, SID of ligand-bound CTB results in the generation of subcomplexes with a ligand distribution reflective of two subunits contributing to each ligand binding site. SID thus has potential application in localizing sites of small ligand binding for multisubunit protein–ligand complexes.



Understanding how ligands are bound within protein complexes is critical in exploring important cellular processes and in rationalizing the structural basis of protein–drug interactions.^{1,2} Structural biology techniques like X-ray crystallography, nuclear magnetic resonance spectroscopy, and cryo-electron microscopy are suitable for obtaining information on subunit–ligand interactions at an atomic level,^{3–5} but sample preparation and data analysis are challenging and can limit their general usability. In many cases, it is desirable to obtain less detailed information at a higher speed and lower cost to allow for the processing of large sample numbers, for instance in ligand screening applications. Native mass spectrometry (MS) is an already well-established and powerful technique to rapidly assess the stoichiometry of protein–ligand complexes ionized from aqueous, nondenaturing solution by nano electrospray ionization (nESI).^{6–17} Separation in the m/z space allows for determination of the distribution of ligand-bound protein ions,¹⁸ which can then be individually isolated with a quadrupole mass filter and probed in the gas phase by one or a combination of dissociation techniques. Two options are to use UV-photodissociation or electron-based activation methods to generate covalent fragments.^{19,20} Comparing the covalent fragmentation patterns of apo and ligand-bound protein complexes can help to locate ligand interaction sites and can provide information on the binding site at the residue level.^{19,21–26} However, these techniques are limited to small protein complexes as the chance of signal overlap increases with the number of different fragment ions, making assignments challenging even when using Fourier transform instruments that provide ultrahigh mass resolution and mass measurement accuracy.²⁷ Furthermore, partial ligand loss

during covalent fragmentation can complicate the analysis for ligand-bound protein complexes and result in the co-occurrence of apo and ligand-bound covalent fragment ion series. Consequently, we set out to explore complementary methods suitable for locating ligand binding sites in multi-subunit protein–ligand complexes without the need to generate covalent fragments. Collision-induced dissociation (CID) is the most commonly used dissociation technique in MS/MS and can also be used for the disruption of noncovalent interactions. It has been successfully employed to probe protein complex stability in the gas phase.^{28–30} However, the underlying multiple collision, slow energy deposition mechanism frequently results in structural rearrangements prior to complex dissociation, generating highly charged, unfolded monomer and complementary $(n - 1)$ mer.^{31,32} In contrast, surface-induced dissociation (SID), in which ions experience a single fast collision with a solid surface, shows promise as a structural probing method presumably due to the rapid, high-energy transfer step, which prevents significant structural rearrangement prior to complex dissociation.^{31,33} SID typically results in symmetrically charged subcomplexes reflective of the quaternary structures of native protein complexes. In this work, we examined the utility of SID in probing protein–ligand complex structures compared to CID. We chose to study two biomedically important homopentameric protein complexes in detail. Those are C-reactive protein (CRP) and cholera toxin B

Received: July 21, 2018

Accepted: October 9, 2018

Published: October 9, 2018

(CTB). Human CRP is a classical member of the ancient innate immune mediator pentraxin family. The Ca^{2+} -mediated binding of the phosphatidylcholine headgroup phosphocholine (PC) to CRP results in the activation of the complement system.³⁴ The ligand binding sites are within each subunit (Figure 1A).³⁵ CTB from *Vibrio cholera* is part of Cholera

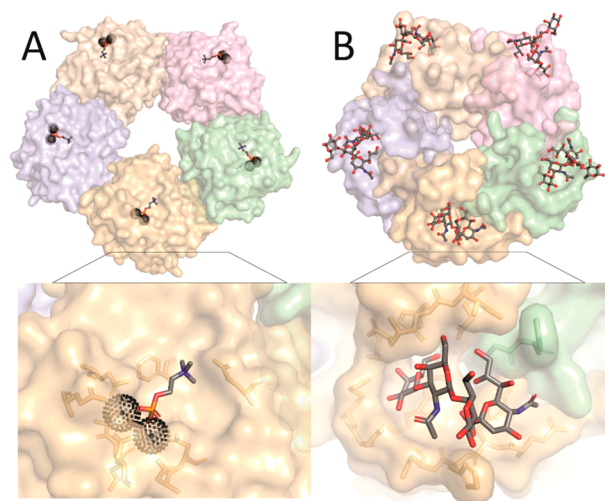


Figure 1. Ligand binding in CRP (1B09) and CTB (2CHB). Overall surface presentation and binding pocket of (A) CRP and (B) CTB. Ligands PC and GM1s are shown in stick presentation, and Ca^{2+} ions are shown as black spheres. Subunits are individually colored. Residues within 4 Å of the ligand are shown as sticks. The ligand binding pocket of CRP is within each subunit, whereas the ligand binding pocket of CTB is composed of residues from two adjacent subunits.

toxin. It binds to the headgroup of the GM1 ganglioside receptor (GM1s) to manifest cell intoxication.³⁶ The ligand binding sites are located between the subunits near the subunit–subunit interface (Figure 1B).^{37–39} The differences in ligand binding for CRP and CTB make them suitable model systems to evaluate SID as a tool to distinguish different modes of ligand binding interactions in protein complexes.

EXPERIMENTAL SECTION

Chemicals and Proteins. Calcium acetate, phosphocholine (PC) chloride calcium salt tetrahydrate, ammonium acetate, and triethylammonium acetate solution were purchased from Sigma-Aldrich (St. Louis, MO). The sodium salt of the pentasaccharide Gal β 1-3GalNAc β 1-4(Neu5Ac- α 2-3)-Gal β 1-4Glc (GM1s) was obtained from Elicityl (Crolles, France). Recombinant human C-reactive protein (CRP) produced in *E. coli* was purchased from Calbiochem (EMD Biosciences, Inc., San Diego, CA) and Sigma-Aldrich (St. Louis, MO). Cholera toxin B (CTB) was purchased from Sigma-Aldrich (St. Louis, MO).

Ligand Titration to CRP. CRP pentamer was buffer exchanged into 200 mM ammonium acetate twice using Micro Bio-Spin 6 columns (Bio-Rad, Hercules, CA.). Different amounts of Ca^{2+} or PC-2 Ca^{2+} were added to 1 μM protein, and mass spectra were recorded after 10 min incubation at room temperature.

Preparation of Ligand-Bound CRP for CID and SID Experiments. CRP pentamer was buffer exchanged into 200 mM ammonium acetate twice using Micro Bio-Spin 6 columns (Bio-Rad, Hercules, CA). Then 200 μM PC and 400 μM Ca^{2+}

were added to 1 μM protein, and 1 M triethylammonium acetate (TEAA) was added to a final concentration of 50 mM prior to MS analysis.

Preparation of Ligand-Bound CTB for CID and SID Experiments. First 1 μM CTB pentamer was mixed with a 50-fold excess of GM1s (10 GM1s per 1 CTB monomers). GM1s-bound CTB was buffer exchanged into 200 mM ammonium acetate twice using Micro Bio-Spin 6 columns (Bio-Rad, Hercules, CA). Then 1 M triethylammonium acetate (TEAA) was added to a final concentration of 50 mM prior to MS analysis.

High-Resolution MS. Experiments were performed on an Exactive Plus EMR Orbitrap mass spectrometer (Thermo Fisher Scientific, Bremen, Germany) modified as described in depth elsewhere.^{40–42} Briefly, the instrument was modified with a quadrupole mass filter from a Q Exactive instrument, driven by a modified rf power supply producing a resonance frequency of 284 kHz to enable precursor selection up to approximately 20 000 m/z . An SID cell was installed in place of the octupole between the selection quadrupole and the C-trap (VanAernum, Z. L.; Gilbert, J. D.; Belov, M. E.; Makarov, A. A.; Horning, S. R.; Wysocki, V. H., in preparation). Voltages were supplied to the SID cell and the C-trap offset via a dc power supply (Ardara Technologies, Ardara, PA) and controlled by Tempus Tune software (Ardara Technologies, Ardara, PA).

The ion source temperature was set to 275 °C, and proteins were ionized by nanoESI with spray voltages of 0.9–1.2 kV, using in-house pulled glass capillaries. In-source CID was set to 0 V, and HCD was set to 1 V for CTB samples. In-source CID was set to 10 V, and HCD was set to 10 V for CRP samples. Source temperature and slight collisional activation were necessary to help desolvate and fully resolve all CRP-ligand species, enabling quadrupole selection and activation of a single ligand-bound species. Transfer ion optic voltages were tuned to optimize ion transmission over the m/z range of interest, while being careful not to unintentionally heat the ions. The mass range was set to m/z 600–16 000. The HCD cell was maintained at a pressure that was indirectly measured between 5 and 8.5×10^{-10} mbar by the ultrahigh vacuum (UHV) gauge near the Orbitrap. Resolution (at m/z 200) was set to 35 000 for all experiments. The instrument was mass calibrated using Thermo Scientific Pierce LTQ Velos ESI Positive Ion Calibration Solution and CsI solution as separate calibrations. SID was performed by applying a repulsive voltage to the front bottom deflector to guide the ions toward the surface for collision and appropriate voltages to the ensuing lenses for ion collection and transmission to the C-trap.

Data Deconvolution and Relative Quantitation. MS data were deconvoluted using Intact Mass software version w2.15-294-gba5daea4b (Protein Metrics Inc., San Carlos, CA).⁴³ Full mass spectra were deconvoluted using the following parameters: minimum difference between peaks: 10, charge vector spacing: 1, baseline radius (m/z): 15, smoothing sigma (m/z): 0.02, spacing (m/z): 0.04, mass smoothing sigma: 3, mass spacing: 0.5, iteration max: 10, for CRP (mass range: 100 000–120 000 Da, charge range: 8–25), and for CTB (mass range: 10 000–65 000 Da, charge range: 4–18). CID and SID (MS/MS) spectra were deconvoluted using the following parameters: minimum difference between peaks: 10, charge vector spacing: 2, baseline radius (m/z): 15, smoothing sigma (m/z): 0.02, spacing (m/z): 0.04, mass smoothing sigma: 3, mass spacing: 0.5, iteration max: 40, for

CRP (mass range: 20 000–120 000 Da, charge range: 8–18), for CTB (mass range: 10 000–65 000 Da, charge range: 2–11). SID CTB spectra were deconvoluted using a beta version of PMI Intact Mass that allows multiple “KnownMassDelta” inputs to assist with charge assignment of overlapping oligomeric states. The known mass differences were 11 605, 12 604, and 13 603 Da, corresponding to protein, protein plus one ligand, and protein plus two ligands. A charge state for an m/z peak that places another m/z peak at a known mass difference is favored over a charge state with no such companion peak.

Relative quantitation of ligand-bound products for CID spectra was accomplished by integrating the peak area of each ligated species in deconvoluted mass space using Intact Mass. For CID of CTB products, water loss and ligand fragment products were included with the appropriate ligated state. For example: the mass area of the tetramer with four GM1s was combined with the tetramer containing three full GM1s and one partially fragmented GM1s. It was observed that Intact Mass software had trouble determining relative quantities of subcomplexes produced by SID. We believe that this is due to the fact that SID produces predominantly symmetrically charged products and therefore results in overlapping oligomeric states in m/z space (e.g., 2+ monomer, 4+ dimer, 6+ trimer, and 8+ tetramer as observed for SID of CTB). Furthermore, the narrow average charge state distribution as well as charge-stripping prior to dissociation complicate quantification when assuming a Gaussian charge state distribution for the generated SID products. As a result, Intact Mass often over- or underestimated the quantity of subcomplexes produced by SID. For instance, the quantity of dimer and trimer for SID of 18+ CRP is likely overestimated relative to monomer (Figure S4). Note that the mass spectra on the left of Figure S4 were manually labeled while the deconvoluted spectra on the right were labeled by the software. For this reason, instead of using Intact Mass for the relative quantitation of ligand-bound subcomplexes, we used the height of subcomplex ion signals that do not overlap in m/z space. Height ratios for apo and ligand-bound subcomplexes were calculated for each charge state indicated in Table S1 and subsequently averaged.

RESULTS AND DISCUSSION

Ligand Binding to CRP and CTB. Addition of 200 μM PC and 400 μM Ca^{2+} to CRP results in a change in mass of the most abundant species from 115 138.6 \pm 1.7 Da (expected for apo CRP: 115 139.2) to 116 436.9 \pm 0.4 Da. The increase by 1298.3 Da corresponds to the binding of 5 PC and 10 Ca^{2+} when taking into account the deprotonation of PC and the side chains of Glu81, Glu138, and Glu147 in CRP upon ligand binding ($5 \times \text{PC} + 10 \times \text{Ca}^{2+} - 25 \times \text{H}^+ = 1296.3$ Da) (Figure 2A).³⁵ We confirmed by titration experiments that 5 PC and 10 Ca^{2+} are bound on average under ligand saturating conditions, consistent with the known specificity of ligand binding, with a small proportion of CRP with less than 5 PC and 10 Ca^{2+} as well as some nonspecifically bound PC and Ca^{2+} being detectable. (Figure S1). For CTB, binding of GM1s (sugar headgroup of GM1) results in a change in mass for the most abundant species from 58 025.2 \pm 0.1 Da (expected for apo CTB: 58 025.8 Da) to 63 019.2 \pm 0.2 Da. The difference of 4994.0 Da corresponds to the binding of 5 protonated GM1s to the CTB pentamer ($5 \times \text{GM1s} + 5 \times \text{H}^+ = 4994.4$ Da) (Figure 2B). Consistent with data from the Klassen

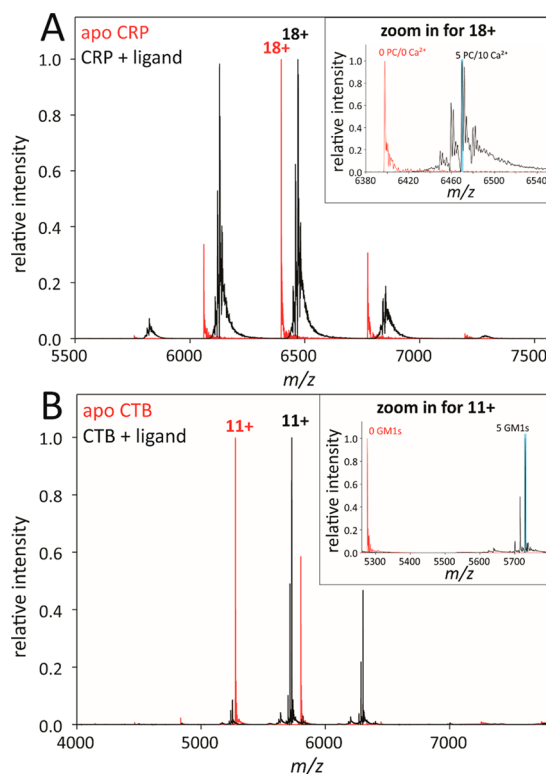


Figure 2. Overlay of apo and ligand-bound protein complex mass spectra for (A) CRP and (B) CTB. Highest intensity apo and ligand-bound species (charge state 18+ for CRP and 11+ for CTB) are highlighted as inset. Ligand-bound pentamers selected for CID and SID are emphasized by light blue. Apo and ligand-bound protein complex mass spectra are colored red and black, respectively. Deconvoluted spectra can be found in the Supporting Information along with detailed labeling of all observed species (Figure S3).

group,⁴⁴ the presence of an excess of GM1s results in saturation of the five protein binding sites with no nonspecific carbohydrate binding being detected. In summary, our data suggest that under the conditions used in this investigation, the dominant species formed has all five ligand binding sites occupied within CRP and on CTB, respectively. We subsequently used the quadrupole mass filter to select only the saturated species to probe by CID and SID in order to determine the ability of each activation technique to distinguish between different ligand binding sites (Figure 3).

CID of Ligand-Bound CRP and CTB Does Not Provide Information on Ligand Location. CID of ligand-bound CRP pentamer results in the production of tetramer and monomer. (Figure 3A). No ligand is retained on highly charged monomers (M^{10+} – M^{6+}), and even for the lowest charge state monomer (M^{5+}), the ligand free form is the most abundant. Ligand loss is also observed for the remaining pentamer, with extensive charge stripping resulting from loss of positively charged PC (P^{17+} – P^{14+}). Generated tetramer retains a large amount of PC ligand. The detection of tetramer with up to five PC bound indicates structural rearrangement and/or ligand migration taking place. In the case of CTB, CID also results in the dissociation of pentamer into tetramer and monomer (Figure 3C). No ligand is retained on the monomers, and 2–5 GM1s are detected on the tetramer. Besides ligand loss and ligand migration, a significant amount of [tetramer + ligand – H_2O] due to water loss from the

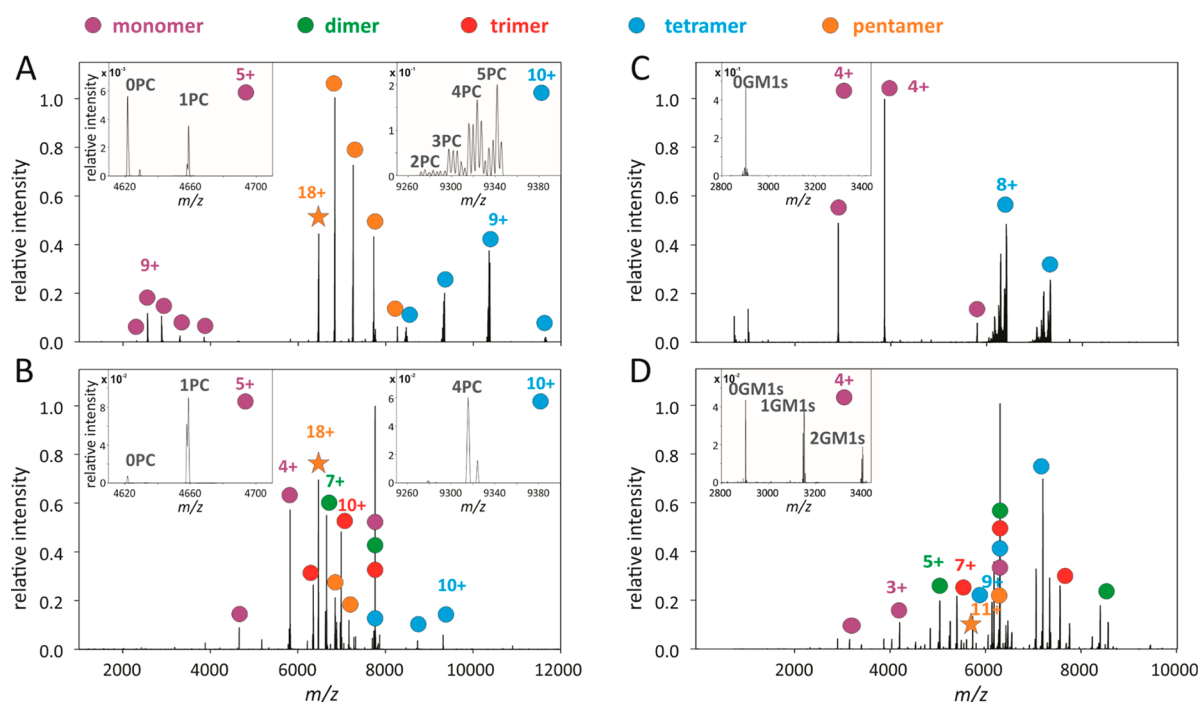


Figure 3. MS/MS of ligand-bound 18+ CRP by (A) CID at 2700 eV and by (B) SID at 630 eV. The distribution of ligands on 5+ monomers and 10+ tetramers is included as inset. MS/MS of ligand-bound 11+ CTB by (C) CID at 2200 eV and by (D) SID at 605 eV. The distribution of ligands on 4+ monomers is magnified and included as inset. * = selected precursor, Charge states are indicated. CID and SID energies were selected to give comparable extent of precursor depletion. Deconvoluted spectra and data for additional CID and SID energies are provided in the Supporting Information (Figures S4 and S5).

GM1s ligand as well as ligand fragments are observed (Figure S2).

Indicated by the ligand distribution on generated tetramer, it is apparent that CID results in ligand loss and ligand migration independent of the initial ligand binding site (binding within CRP subunits/binding between CTB subunits). Furthermore, almost no ligand is retained on the monomer, providing no structural localization of the ligand binding sites based on noncovalent fragments.

SID of Ligand-Bound CRP and CTB Provides Information on Ligand Location. SID of CRP pentamer leads to the dissociation into monomer, dimer, trimer, and tetramer as expected for a cyclic assembly with equal subunit–subunit interactions (Figure 3B). The average charge state of generated monomer closely matches that expected for symmetric charge state partitioning (expected: $18/5 = 3.6$). Almost no ligand-free monomer is observable even for the highest charge state (M^{5+}) generated. The distribution of ligand on the tetramer (TT^{10+}) reflects that expected for 4 binding pockets with predominantly 4 PC and 8 Ca^{2+} bound and a minor proportion of 4 PC and 10 Ca^{2+} bound. SID-generated trimers and dimers predominantly retain three and two PC, respectively, and little ligand-loss is observed. For SID of ligand-bound CTB, all accessible subcomplexes (monomer, dimer, trimer, tetramer) are also generated, the products expected when cleaving two interfaces of a pentamer (Figure 3D).

The generated n -mers show characteristic patterns of $n - 1$, n , and $n + 1$ ligand-bound species. This is consistent with the ligand being bound across adjacent subunits in solution and distributed on either one or the other subunit during dissociation. Based on the CTB crystal structure, GM1s is unequally bound across the subunits. In detail, the ligand

interacts with one subunit via hydrogen bonding to Glu11, His13, Asn90, Lys91, and Glu51 and a solvent-mediated hydrogen bond to Asn14, but only through one solvent-mediated hydrogen bond to Gly33 with the other subunit.³⁷ The relatively high abundance of SID-generated subcomplexes with $n - 1$ and $n + 1$ ligands bound might at least be in part attributed to thermal activation and some background CID, which strongly suggests that the ligand localization and not the detailed interactions between ligand and subunits is the main determinant of the ligand distribution. In fact, the distribution of ligands on the SID products $n - 1$, n , $n + 1$ is close to a 1:2:1 ratio expected for a ligand shared evenly between subunits upon interface cleavage by SID, although the crystal structure clearly indicates that the ligands are not distributed evenly between subunits and may thus indicate local ligand restructuring in the gas phase. A plot with the ligand distribution of SID- and CID-generated subcomplexes is shown in Figure 4. This figure highlights that no information on the initial binding location is retained upon complex dissociation by CID due to ligand rearrangement and restructuring/unfolding. In contrast, the fast energy deposition over a large area due to surface collision significantly increases the chance of retaining ligands bound within subunits while cleaving protein–protein interfaces. This is particularly true for ligands that are tightly bound to a protein via multiple noncovalent interactions. As a matter of future work, we intend to determine how the number and nature of protein–ligand interactions relative to the protein–protein interactions influence the retention of ligands on SID products in more detail.

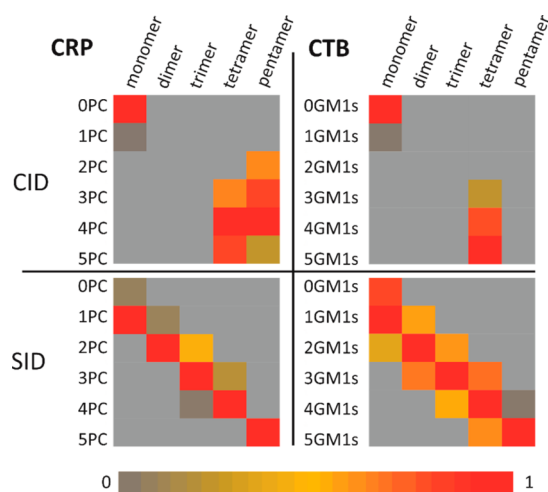


Figure 4. Distribution of ligands on (sub)complexes generated from dissociation of CRP and CTB pentamers by SID and CID, respectively. Nonoverlapping charge states for each oligomeric state were used for relative quantitation of each species. Species differing only by Ca^{2+} in the case of CRP and water in the case of CTB were combined. Data were normalized to 1 for each observed n -mer. Quantification is based on data shown in Figure 3.

CONCLUSION

We have previously shown that complex stability probed by SID can provide indirect evidence for the ligand localization within a protein complex, albeit with insufficient mass resolution to determine the ligand distribution on SID-generated subcomplexes.⁴⁵ Here, we highlight a practical benefit of our SID implementation on an Orbitrap platform (manuscript in preparation) with the ability to directly analyze the ligand distribution of SID-generated subcomplexes, even in cases where the mass of the ligand is very small compared to the mass of the protein complex. This work exemplifies how SID on the Orbitrap platform has potential for the rapid differentiation of ligand binding sites within and between subunits by the acquisition of a single midenergy SID fragmentation spectrum.

ASSOCIATED CONTENT

Supporting Information

The Supporting Information is available free of charge on the ACS Publications website at DOI: 10.1021/acs.analchem.8b03263.

Charge states used for the relative quantitation of ligand-bound subcomplexes produced by SID of CRP and CTB pentamer; titration of ligands to 1 μM CRP pentamer in 200 mM ammonium acetate; ligand distribution observed on CID-generated CTB tetramer; mass spectra and deconvoluted spectra for CRP and CTB with and without ligands bound; mass spectra and deconvoluted spectra for MS/MS of 18+ ligand-bound CRP; mass spectra and deconvoluted spectra for MS/MS of 11+ ligand-bound CTB (PDF)

Spectra data for MS of CRP and CTB with and without ligands bound (XLSX)

MS/MS of 18+ ligand-bound CRP and 11+ ligand-bound CTB (XLSX)

AUTHOR INFORMATION

Corresponding Author

*E-mail: wysocki.11@osu.edu. Phone: +1-614-292-8687.

ORCID

Florian Busch: 0000-0002-4324-6065

Present Addresses

Y.J.: Bruker Daltonics Inc., 61 Daggett Dr., San Jose, California 95134.

J.Y.: Department of Chemistry, Washington University in St. Louis, St. Louis, Missouri 63130.

J.D.G.: Thermo Fisher Scientific Inc., 5350 NE Dawson Creek Dr., Hillsboro, Oregon 97124.

R.S.Q.: Thermo Fisher Scientific Inc., 1400 Northpoint Pkwy., West Palm Beach, Florida 33407.

Author Contributions

[†]F.B., Z.L.V., and Y.J. contributed equally to this work.

Funding

This work was supported by the National Institutes of Health (NIH R01GM113658 to V.H.W.) and the National Science Foundation for instrument development (NSF DBI 1455654 to VHW). F.B. was supported by a fellowship from the German Research Foundation (DFG).

Notes

The authors declare the following competing financial interest(s): M.B. is a founder and part owner of Protein Metrics, Inc. F.B., Z.L.V.A., Y.J., J.Y., J.D.G., R.S.Q. and V.H.W. declare no competing financial interests.

ACKNOWLEDGMENTS

We thank Dr. St John Skilton for support and advice with Protein Metrics and Dr. Mowei Zhou for helpful initial discussions.

REFERENCES

- Robinson, C. V.; Sali, A.; Baumeister, W. *Nature* **2007**, *450*, 973–982.
- Rual, J.-F.; Venkatesan, K.; Hao, T.; Hirozane-Kishikawa, T.; Dricot, A.; Li, N.; Berriz, G. F.; Gibbons, F. D.; Dreze, M.; Ayivi-Guedehoussou, N.; Klitgord, N.; Simon, C.; Boxem, M.; Milstein, S.; Rosenberg, J.; Goldberg, D. S.; Zhang, L. V.; Wong, S. L.; Franklin, G.; Li, S.; et al. *Nature* **2005**, *437*, 1173–1178.
- Ilari, A.; Savino, C. In *Bioinformatics*; Keith, J., Ed.; Humana Press: New York, 2008; pp 63–87.
- Nietlispach, D.; Mott, H.; Stott, K.; Nielsen, P.; Thiru, A.; Laue, E. In *Protein NMR Techniques*; Downing, A. K., Ed.; Humana Press: New York, 2004; pp 255–288.
- Jonic, S.; Vénien-Bryan, C. *Curr. Opin. Pharmacol.* **2009**, *9*, 636–642.
- Loo, J. A. *Int. J. Mass Spectrom.* **2000**, *200*, 175–186.
- Benesch, J. L. P.; Robinson, C. V. *Curr. Opin. Struct. Biol.* **2006**, *16*, 245–251.
- Benesch, J. L. P.; Ruotolo, B. T.; Simmons, D. A.; Robinson, C. V. *Chem. Rev.* **2007**, *107*, 3544–3567.
- Benesch, J. L. P.; Aquilina, J. A.; Ruotolo, B. T.; Sobott, F.; Robinson, C. V. *Chem. Biol.* **2006**, *13*, 597–605.
- Heuvel, R. H. H. v. d.; Heck, A. J. R. *Curr. Opin. Chem. Biol.* **2004**, *8*, 519–526.
- Hall, Z.; Politis, A.; Robinson, C. V. *Structure* **2012**, *20*, 1596–1609.
- Lorenzen, K.; Vannini, A.; Cramer, P.; Heck, A. J. R. *Structure* **2007**, *15*, 1237–1245.
- Damoc, E.; Fraser, C. S.; Zhou, M.; Videler, H.; Mayeur, G. L.; Hershey, J. W. B.; Doudna, J. A.; Robinson, C. V.; Leary, J. A. *Mol. Cell. Proteomics* **2007**, *6*, 1135–1146.

- (14) McCammon, M. G.; Hernández, H.; Sobott, F.; Robinson, C. V. *J. Am. Chem. Soc.* **2004**, *126*, 5950–5951.
- (15) Jones, C. M.; Beardsley, R. L.; Galhena, A. S.; Dagan, S.; Cheng, G.; Wysocki, V. H. *J. Am. Chem. Soc.* **2006**, *128*, 15044–15045.
- (16) Hyung, S.-J.; Robinson, C. V.; Ruotolo, B. T. *Chem. Biol.* **2009**, *16*, 382–390.
- (17) Zhou, M.; Morgner, N.; Barrera, N. P.; Politis, A.; Isaacson, S. C.; Matak-Vinkovic, D.; Murata, T.; Bernal, R. A.; Stock, D.; Robinson, C. V. *Science* **2011**, *334*, 380–385.
- (18) Dyachenko, A.; Gruber, R.; Shimon, L.; Horovitz, A.; Sharon, M. *Proc. Natl. Acad. Sci. U. S. A.* **2013**, *110*, 7235–7239.
- (19) Li, H.; Sheng, Y.; McGee, W.; Cammarata, M.; Holden, D.; Loo, J. A. *Anal. Chem.* **2017**, *89*, 2731–2738.
- (20) O'Brien, J. P.; Li, W.; Zhang, Y.; Brodbelt, J. S. *J. Am. Chem. Soc.* **2014**, *136*, 12920–12928.
- (21) Xie, Y.; Zhang, J.; Yin, S.; Loo, J. A. *J. Am. Chem. Soc.* **2006**, *128*, 14432–14433.
- (22) Yin, S.; Loo, J. A. *J. Am. Soc. Mass Spectrom.* **2010**, *21*, 899–907.
- (23) Li, H.; Wongkongkathep, P.; Van Orden, S.; Ogorzalek Loo, R.; Loo, J. *J. Am. Soc. Mass Spectrom.* **2014**, *25*, 2060–2068.
- (24) Xie, Y.; Zhang, J.; Yin, S.; Loo, J. A. *J. Am. Chem. Soc.* **2006**, *128*, 14432–14433.
- (25) Mehaffey, M. R.; Cammarata, M. B.; Brodbelt, J. S. *Anal. Chem.* **2018**, *90*, 839–846.
- (26) Cammarata, M. B.; Thyer, R.; Rosenberg, J.; Ellington, A.; Brodbelt, J. S. *J. Am. Chem. Soc.* **2015**, *137*, 9128–9135.
- (27) Li, H.; Wolff, J. J.; Van Orden, S. L.; Loo, J. A. *Anal. Chem.* **2014**, *86*, 317–320.
- (28) Samulak, B. M.; Niu, S.; Andrews, P. C.; Ruotolo, B. T. *Anal. Chem.* **2016**, *88*, 5290–5298.
- (29) Eschweiler, J. D.; Martini, R. M.; Ruotolo, B. T. *J. Am. Chem. Soc.* **2017**, *139*, 534–540.
- (30) Dixit, S. M.; Polasky, D. A.; Ruotolo, B. T. *Curr. Opin. Chem. Biol.* **2018**, *42*, 93–100.
- (31) Beardsley, R. L.; Jones, C. M.; Galhena, A. S.; Wysocki, V. H. *Anal. Chem.* **2009**, *81*, 1347–1356.
- (32) Popa, V.; Trecroce, D. A.; McAllister, R. G.; Konermann, L. J. *Phys. Chem. B* **2016**, *120*, 5114–5124.
- (33) Zhou, M.; Dagan, S.; Wysocki, V. H. *Angew. Chem., Int. Ed.* **2012**, *51*, 4336–4339.
- (34) Volanakis, J. E.; Narkates, A. J. *J. Immunol.* **1981**, *126*, 1820–1825.
- (35) Thompson, D.; Pepys, M. B.; Wood, S. P. *Structure* **1999**, *7*, 169–177.
- (36) Lencer, W. I.; Tsai, B. *Trends Biochem. Sci.* **2003**, *28*, 639–645.
- (37) Merritt, E. A.; Sarfaty, S.; Akker, F. V. D.; L'Hoir, C.; Martial, J. A.; Hol, W. G. J. *Protein Sci.* **1994**, *3*, 166–175.
- (38) Merritt, E. A.; Sarfaty, S.; Jobling, M. G.; Chang, T.; Holmes, R. K.; Hirst, T. R.; Hol, W. G. *Protein Sci.* **1997**, *6*, 1516–1528.
- (39) Merritt, E. A.; Kuhn, P.; Sarfaty, S.; Erbe, J. L.; Holmes, R. K.; Hol, W. G. J. *J. Mol. Biol.* **1998**, *282*, 1043–1059.
- (40) Rose, R. J.; Damoc, E.; Denisov, E.; Makarov, A.; Heck, A. J. *Nat. Methods* **2012**, *9*, 1084–1086.
- (41) Rosati, S.; Rose, R. J.; Thompson, N. J.; van Duijn, E.; Damoc, E.; Denisov, E.; Makarov, A.; Heck, A. J. *Angew. Chem., Int. Ed.* **2012**, *51*, 12992–12996.
- (42) Dyachenko, A.; Wang, G.; Belov, M.; Makarov, A.; de Jong, R. N.; van den Bremer, E. T.; Parren, P. W.; Heck, A. J. *Anal. Chem.* **2015**, *87*, 6095–6102.
- (43) Bern, M. J. *Proteome Res.* **2018**, *17*, 1216–1226.
- (44) Zhang, Y.; Deng, L.; Kitova, E.; Klassen, J. J. *J. Am. Soc. Mass Spectrom.* **2013**, *24*, 1573–1583.
- (45) Quintyn, R. S.; Yan, J.; Wysocki, V. H. *Chem. Biol.* **2015**, *22*, 583–592.